Nuclear dipole polarizability from mean-field models constrained by chiral effective field theory

Zhen Zhang*, Yeunhwan Lim†, Jeremy W. Holt‡, and Che Ming Ko§
Cyclotron Institute and Department of Physics and Astronomy,
Texas A&M University, College Station, Texas 77843, USA
(Dated: March 6, 2017)

Using extended Skyrme interactions that are constructed from fitting both the binding energies of finite nuclei and the equation of state of asymmetric nuclear matter from chiral two and three-body forces, we study the electric dipole polarizabilities of ^{48}Ca, ^{68}Ni, ^{120}Sn, and ^{208}Pb in the random-phase approximation. We find that the theoretical predictions are in good agreement with experimentally measured values without additional fine tuning of the Skyrme interactions, thus confirming the usefulness of these extended Skyrme interactions in studying the properties of nuclei. We also study the correlation between the electric dipole polarizability and the neutron skin thickness.

PACS numbers: 24.30.Cz,21.60.Jz,21.30.Fe

arXiv:1703.00866v2 [nucl-th] 3 Mar 2017

I. INTRODUCTION

The nuclear electric dipole polarizability $\alpha_{\rm D}$, which is proportional to the inverse energy-weighted sum of the dipole response of a nucleus to an external electric field, has attracted much attention recently due to its strong correlation with neutron skin thicknesses, the density dependence of the nuclear symmetry energy [1–9], and the properties of neutron stars [10–12]. The electric dipole response is dominated by the nuclear isovector giant dipole resonance (IVGDR), which is the oldest known nuclear collective excitation and has been extensively studied both theoretically and experimentally [13–16]. It is well known from theoretical studies based on various models that the properties of IVGDR, in which neutrons oscillate against protons in a nucleus, is affected by the density dependence of the nuclear symmetry energy [17–21].

Experimentally, the electric dipole strength distributions in ^{48}Ca [22], ^{120}Sn [23], and ^{208}Pb [24] have recently been accurately measured at the Research Center for Nuclear Physics (RCNP) from proton inelastic scattering experiments at forward angles, while that of ^{68}Ni has been investigated at GSI using Coulomb excitations in inverse kinematics and measuring the invariant mass in the one- and two-neutron decay channels [25]. Recently, ab initio calculations based on chiral effective field theory interactions have been successful at describing $\alpha_{\rm D}$ in medium-mass nuclei [26, 27], but the description of the dipole response of heavy nuclei remains a challenge. Therefore, nuclear energy density functionals are still the most widely-used approach to explore the nuclear equation of state (EOS) from the electric dipole response.

In the present work, we study the dipole response of ^{48}Ca, ^{68}Ni, ^{120}Sn, and ^{208}Pb within the random-phase approximation (RPA) employing three new extended Skyrme interactions [28] that have been constructed by fitting both the binding energies of finite nuclei and the equation of state of asymmetric nuclear matter predicted by chiral two- and three-body forces. The calculated electric dipole polarizabilities are in good agreement with existing experimental values. Furthermore, we investigate the correlation between $\alpha_{\rm D}$ and the neutron skin thickness.

The paper is organized as follows. In Section II, we explain in detail the extended Skyrme interactions that are used in the present work to compute the electric dipole response of ^{48}Ca, ^{68}Ni, ^{120}Sn, and ^{208}Pb. In Section III, we describe the random-phase approximation framework employed in our calculations, and in Section IV we present results and discussions for the isovector dipole response, electric dipole polarizability, and neutron skin thicknesses of selected nuclei from the three extended Skyrme mean field models. We end with a summary in Section V.

II. EXTENDED SKYRME INTERACTIONS FROM CHIRAL EFFECTIVE THEORY

In Ref. [28], Lim and Holt constructed extended Skyrme interactions constrained by the asymmetric nuclear matter equation of state from chiral two and three-nucleon forces [29, 30]. In contrast to previous works [31, 32] imposing constraints on mean field models from low-density neutron matter, in Ref. [28] the full density-dependence of the asymmetric matter equation of state was used in the χ^2 minimization function. In these calculations the chiral two-body force was treated at next-to-next-to-next-to-leading order (N3LO) in the chiral power counting, while the three-body force was treated at N2LO. Three different choices of the momentum-space cutoff were considered $\{\Lambda = 414,\ 450$ and 500 MeV$\}$, and the unknown low-energy constants associated with short-distance dynamics were fitted [33–36] in each case to nucleon-nucleon scattering phase shifts and deuteron

*zhenzhang@comp.tamu.edu
†ylim@tamu.edu
‡holt@physics.tamu.edu
§ko@comp.tamu.edu

properties (in the case of the nucleon-nucleon interaction) as well as the binding energy and beta-decay lifetime of ^{3}H (in the case of the three-nucleon force). To fix the gradient contributions to the energy density functional, the extended Skyrme interactions were also fitted to reproduce the binding energies of 7 doubly-closed-shell nuclei: ^{16}O, ^{40}Ca, ^{48}Ca, ^{56}Ni, ^{100}Sn, ^{132}Sn, and ^{208}Pb. The conventional Skyrme interaction [37] was found to be inadequate to describe the density-dependent equation of state from chiral effective field theory, leading the authors of Ref. [28] to include an additional density-dependent and momentum-independent t_4 term. The extended Skyrme interactions employed in the present study therefore have the following form:

$$\begin{aligned} v(\boldsymbol{r}_1,\boldsymbol{r}_2) &= t_0(1+x_0P_\sigma)\delta(\boldsymbol{r}_1-\boldsymbol{r}_2) \\ &+\frac{1}{2}t_1(1+x_1P_\sigma)[\boldsymbol{k}'^2\delta(\boldsymbol{r}_1-\boldsymbol{r}_2)+\text{c.c.}] \\ &+t_2(1+x_2P_\sigma)\boldsymbol{k}'\cdot\delta(\boldsymbol{r}_1-\boldsymbol{r}_2)\boldsymbol{k} \\ &+\frac{1}{6}t_3(1+x_3P_\sigma)\rho^\alpha\left(\frac{\boldsymbol{r}_1+\boldsymbol{r}_2}{2}\right)\delta(\boldsymbol{r}_1-\boldsymbol{r}_2) \\ &+\frac{1}{6}t_4(1+x_4P_\sigma)\rho\left(\frac{\boldsymbol{r}_1+\boldsymbol{r}_2}{2}\right)\delta(\boldsymbol{r}_1-\boldsymbol{r}_2) \\ &+iW_0(\boldsymbol{\sigma}_1+\boldsymbol{\sigma}_2)\cdot[\boldsymbol{k}'\times\delta(\boldsymbol{r}_1-\boldsymbol{r}_2)\boldsymbol{k}], \end{aligned} \quad (1)$$

where $\boldsymbol{\sigma}_i$ is the Pauli spin operator, $P_\sigma=(1+\boldsymbol{\sigma}_1\cdot\boldsymbol{\sigma}_2)/2$ is the spin-exchange operator, $\boldsymbol{k}=-i(\boldsymbol{\nabla}_1-\boldsymbol{\nabla}_2)/2$ is the relative momentum operator, and $\boldsymbol{k}'$ is the conjugate operator of $\boldsymbol{k}$ acting on the left. Note that contributions of the t_4 term on the properties of finite nuclei and nuclear matter can be easily obtained from those of the t_3 term by replacing t_3, x_3 and α with t_4, x_4 and unity, respectively.

In Table I, we show various characteristic properties of bulk nuclear matter predicted by Hartree-Fock calculations using the three extended Skyrme interactions Skχ414, Skχ450 and Skχ500. In particular, the saturation density ρ_0, the binding energy per nucleon in symmetric nuclear matter $E_0(\rho_0)$, the incompressibility K_0, as well as the magnitude $E_{\rm sym}(\rho_0)$ and density slope L of the nuclear symmetry energy at saturation density are all consistent with empirical values (see e.g., Ref. [38]). In addition, we list in Table I the isoscalar and isovector effective masses $m^*_{s,0}$ and $m^*_{v,0}$ at ρ_0 [37]:

$$\frac{1}{m^*_{s,0}} = \frac{1}{m}+\frac{1}{8}[3t_1+t_2(5+4x_2)]\rho_0, \quad (2)$$

$$\frac{1}{m^*_{v,0}} = \frac{1}{m}+\frac{1}{4}[t_1(2+x_1)+t_2(2+x_2)]\rho_0, \quad (3)$$

where $m=939$ MeV is the bare nucleon mass. Using the $m^*_{s,0}$ and $m^*_{v,0}$, the nucleon effective mass in asymmetric nuclear matter at total baryon number density ρ can be expressed as

$$\frac{m}{m^*_q}=1-\frac{\rho}{\rho_0}+\frac{2\rho_q}{\rho_0}\frac{m}{m^*_{s,0}}+\frac{\rho-2\rho_q}{\rho_0}\frac{m}{m^*_{v,0}}, \quad (4)$$

TABLE I: Properties of infinite nuclear matter from the Skχ414, Skχ450 and Skχ500 mean field models.

	Skχ414	Skχ450	Skχ500
ρ_0 (fm^{-3})	0.1697	0.1562	0.1679
E_0 (MeV)	-16.199	-15.926	-15.990
K_0 (MeV)	243.19	239.52	238.16
$E_{\rm sym}(\rho_0)$ (MeV)	32.3	30.6	29.1
L (MeV)	51.9	42.05	40.7
$m^*_{s,0}/m$	1.07	1.01	1.09
$m^*_{v,0}/m$	1.06	0.95	1.37

with $q=n,p$, and $\rho_n(\rho_p)$ being the neutron (proton) density.

In the Skyrme-Hartree-Fock (SHF) model, the isovector effective mass is related to the enhancement factor κ of the Thomas-Reiche-Kuhn sum rule for the IVGDR [39]:

$$\begin{aligned}\kappa &= \frac{mA}{4NZ}\left[t_1\left(2+x_1\right)+t_2\left(2+x_2\right)\right]\int\rho_n\rho_p d^3r, \\ &= \frac{A}{NZ}\left(\frac{m}{m^*_{v,0}}-1\right)\int\frac{\rho_n\rho_p}{\rho_0}d^3r, \end{aligned} \quad (5)$$

where Z, N and A are the proton, neutron and total nucleon numbers, respectively. In particular, we have $(1+\kappa)=m/m^*_{v,0}$ in symmetric nuclear matter at $\rho=\rho_0$.

III. ISOVECTOR DIPOLE RESPONSE AND RANDOM-PHASE APPROXIMATION

The dipole response of a nucleus can be calculated in the random-phase approximation using the dipole operator

$$\hat{F}=\frac{N}{A}\sum_{i=1}^{Z}r_iY_{1\rm M}(\hat{r}_i)-\frac{Z}{A}\sum_{i=1}^{N}r_iY_{1\rm M}(\hat{r}_i), \quad (6)$$

where r_i is the nucleon's radial coordinate and $Y_{1\rm M}(\hat{r}_i)$ is the corresponding spherical harmonic function. In the RPA method, the isovector dipole strength function is evaluated as

$$S(E)=\sum_\nu|\langle\nu\|\hat{F}\|\tilde{0}\rangle|^2\delta(E-E_\nu), \quad (7)$$

where $|\tilde{0}\rangle$ is the RPA ground state, and $|\nu\rangle$ is the RPA excited state with E_ν being its energy. Defining the moments of the strength function as

$$m_k=\int dEE^kS(E)=\sum_\nu|\langle\nu\|\hat{F}\|\tilde{0}\rangle|^2E^k_\nu, \quad (8)$$

the electric dipole polarizability α_D can then be calculated according to

$$\alpha_D=\frac{8\pi}{9}e^2\int dEE^{-1}S(E)=\frac{8\pi}{9}e^2m_{-1}. \quad (9)$$

TABLE II: Experimental data for the electric dipole polarizabilities $\alpha_{\rm D}$ (in units of fm^3) for ^{48}Ca [22], ^{68}Ni [25], ^{120}Sn [23], and ^{208}Pb [24] together with the results of RPA calculations using the Skχ414, Skχ450 and Skχ500 extended Skyrme parametrizations.

	Expt.	Skχ414	Skχ450	Skχ500
^{48}Ca	2.07(22)	2.28	2.44	2.33
^{68}Ni	3.88(31)	3.93	4.22	3.99
^{120}Sn	8.59(36)	8.82	9.50	9.06
^{208}Pb	19.6(6)	19.08	20.55	19.66

In the present work, we extend the Skyrme-RPA code by Colo *et al.* [39] to include the t_4 term and use it to calculate the electric dipole polarizabilities of ^{48}Ca, ^{68}Ni, ^{120}Sn, and ^{208}Pb. As pointed out in Ref. [5], to compare the RPA results with experiment, the experimentally extracted values of $\alpha_{\rm D}$ for ^{120}Sn [23] and ^{208}Pb [24] need to be corrected by subtracting the contributions from quasi-deuteron excitations [40, 41], while that of ^{68}Ni [26] should be modified by including the corrections from the extrapolated low-energy and high-energy regions. The corrected experimental data are shown in Table II.

IV. RESULTS AND DISCUSSIONS

In Fig. 1, we show the isovector dipole transition strength functions for ^{208}Pb obtained from the RPA calculations using the three extended Skyrme interactions Skχ414, Skχ450 and Skχ500. Here the curves are obtained by smearing the RPA results with a Lorentzian function whose width is taken to reproduce the experimental IVGDR width ($\Gamma = 4.07$ MeV [42]). For comparison, the experimental peak energy $E_x = 13.43$ MeV [42] of the IVGDR in ^{208}Pb is shown as the vertical dashed line. It can be seen that the three interactions, especially Skχ500, predict too low peak energies E_x compared with the experimental value. The centroid energy of the IVGDR can be estimated by [18, 21]

$$E_x = \sqrt{\frac{m_1}{m_{-1}}}, \tag{10}$$

and for the three extended Skyrme interactions Skχ414, Skχ450 and Skχ500, their values are 12.1, 12.2 and 10.9 MeV, respectively.

While the inverse energy weighted sum rule m_{-1} is related to the electric dipole polarizability via Eq. (9), the energy weighted sum rule m_1 depends inversely on the isovector effective mass at saturation density $m^*_{v,0}$ in the standard SHF model [43]. The latter can be understood by the fact that the m_1 can be expressed as [39]

$$m_1 = \frac{9}{4\pi}\frac{1}{2m}\frac{NZ}{A}(1+\kappa), \tag{11}$$

where the factor κ is inversely proportional to $m^*_{v,0}$ (see Eq. (5)). Since the t_4 term is momentum independent,

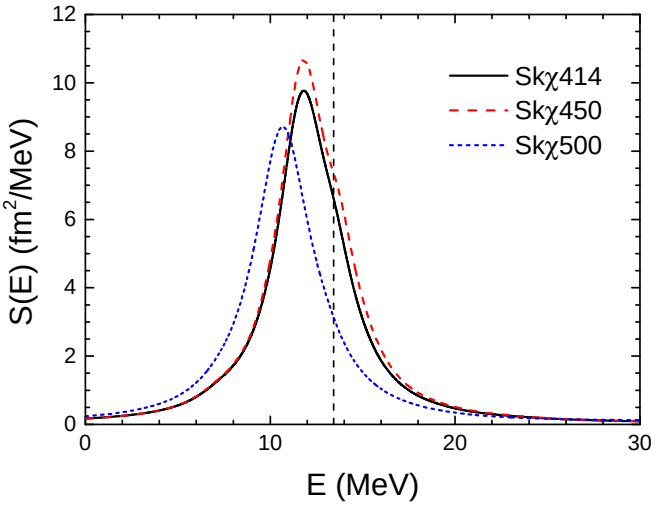

FIG. 1: (Color online) Strength function of the IVGDR in ^{208}Pb obtained from RPA calculations using Skχ414, Skχ450 and Skχ500. The vertical black dash line indicates the measured peak energy [42].

including it in the Skyrme interaction does not affect the relation between m_1 and $m^*_{v,0}$. Therefore, given the large values (see Table I) of $m^*_{v,0}$ predicted by the three extended Skyrme interactions, especially Skχ500, it is expected that imposing constraints on the nucleon effective mass from chiral effective theory [44–47] or macroscopic Skyrme energy density functionals [43] would improve the description of the IVGDR peak energy, and this could be pursued in the future.

Fig. 2 exhibits the electric dipole polarizabilities of ^{48}Ca, ^{68}Ni, ^{120}Sn, and ^{208}Pb predicted by the Skχ414, Skχ450, and Skχ500 mean field models together with the experimental results [22–25] (detailed numerical values are listed in Table II). We find that while Skχ414 and Skχ500 well reproduce the experimental data of the electric dipole polarizability, the predictions of Skχ450 are slightly larger than the experimental values. In the case of ^{48}Ca, we observe that the results are consistent with recent ab initio calculations [26] of the dipole polarizability from chiral effective field theory. We would like to point out that we have calculated the electric dipole polarizability by using discrete RPA peaks because the $1p-1h$ RPA cannot give rise to the spreading width of nuclear giant resonances observed in experiments. Including the spreading width, which can be done by taking into account the coupling of 1p-1h states with more complicated multi-particle–multi-hole configurations, is expected to reduce the calculated α_D slightly. This can be seen by smearing the RPA peaks using the Lorentzian function with a certain width. In the case of only one Lorentzian function of width Γ, the electric dipole polarizability is at most reduced by [5]

$$\Delta\alpha_{\rm D} \sim -\alpha_{\rm D}\frac{\Gamma^2}{4E_x^2}. \tag{12}$$

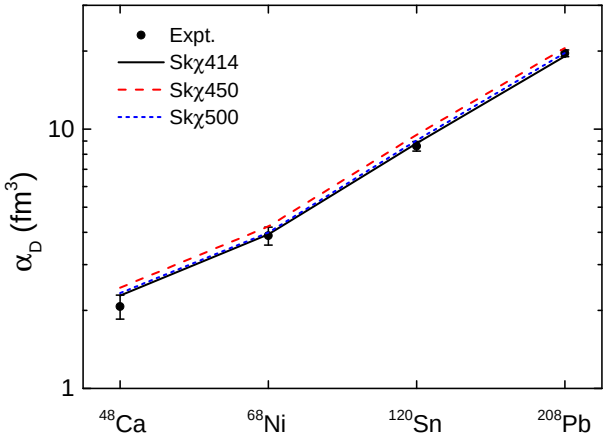

FIG. 2: (Color online) Electric dipole polarizabilities of ^{48}Ca, ^{68}Ni, ^{120}Sn, and ^{208}Pb predicted by Skχ414, Skχ450 and Skχ500. For comparison, experimental data [22–25] are shown as black solid circles.

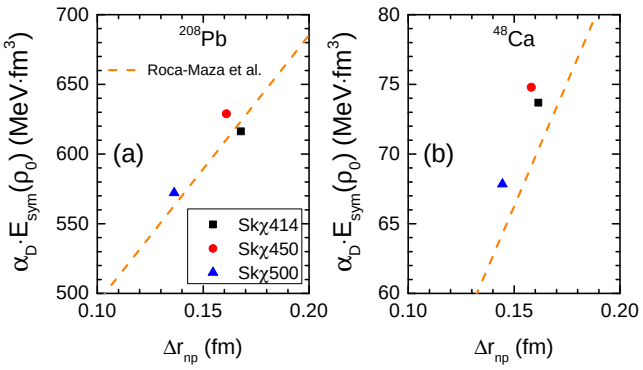

FIG. 3: (Color online) Electric dipole polarizabilities $\alpha_{\rm D}$ times the symmetry energy at saturation density, $E_{\rm sym}(\rho_0)$, against the neutron skin thickness in ^{208}Pb (a) and ^{48}Ca (b) predicted by Skχ414, Skχ450 and Skχ500. Orange dashed lines indicate the linear fits to predictions of various representative energy density functionals by Roca-maza *et al.* [3, 5], i.e., $\alpha_{\rm D}E_{\rm sym}(\rho_0) = 201 + 1922\Delta r_{np}$ for ^{208}Pb and $\alpha_{\rm D}E_{\rm sym}(\rho_0) = 13 + 355\Delta r_{np}$ for ^{48}Ca.

According to this formula, using the experimental value of the peak energy (13.43 MeV) and width (4.07 MeV) of the IVGDR [42], we estimate that the reduction should be less than about 0.45 fm^3 ($\sim 2\%$) for ^{208}Pb. Taking account of this correction, the predictions of Skχ450 would be in better agreement with the experimental values.

In Refs. [3, 5], analyses of RPA calculations using various energy density functionals have revealed that there exists a strong linear correlation between the neutron skin thickness Δr_{np} and the product of the electric dipole polarizability $\alpha_{\rm D}$ and the symmetry energy at saturation density $E_{\rm sym}(\rho_0)$. Shown in Fig. 3 is the product $\alpha_{\rm D}E_{\rm sym}(\rho_0)$ against the neutron skin thickness in ^{48}Ca and ^{208}Pb predicted by the Skχ414, Skχ450 and Skχ500 mean field models. For comparison, the linear fits by Roca-Maza *et al.* [3, 5] to the predictions from a representative set of energy density functionals, i.e.,

$$\alpha_{\rm D}E_{\rm sym}(\rho_0) = \begin{cases} 13 + 355\Delta r_{np}, & \text{for } ^{48}\text{Ca}; \\ 301 + 1922\Delta r_{np}, & \text{for } ^{208}\text{Pb}; \end{cases} \quad (13)$$

with Pearson correlation coefficients of 0.84 and 0.97, respectively, are shown as orange dashed lines. In the above equations, $E_{\rm sym}(\rho_0)$, $\alpha_{\rm D}$, and Δr_{np} are expressed in units of MeV, fm^3, and fm, respectively. It is seen that the results of the three extended Skyrme interactions in general lie along the linear fits, especially for ^{208}Pb. For ^{48}Ca, the deviation between the present results and the linear fit of Roca-Maza *et al.* is understandable because of the weaker correlation.

The predicted neutron skin thicknesses of ^{48}Ca and ^{208}Pb from the three interactions Skχ414, Skχ450 and Skχ500 considered in the present work are given respectively by

$$\Delta r_{np}(^{48}\text{Ca}): \ 0.162, 0.158, 0.145 \text{ fm},$$
$$\Delta r_{np}(^{208}\text{Pb}): \ 0.168, 0.161, 0.136 \text{ fm}.$$

We find that the predicted results for ^{208}Pb are in very good agreement with the constraint $\Delta r_{np} = 0.15 \pm 0.03 \ (\text{stat.})^{+0.01}_{-0.03} \ (\text{sys.})$ fm extracted from coherent pion photoproduction cross sections [48], and are also consistent with the constraint $\Delta r_{np} = 0.302 \pm 0.175 \ (\text{exp}) \pm 0.026 \ (\text{model}) \pm 0.005 \ (\text{strange})$ fm [49] extracted from the parity-violating asymmetry measurement in the Lead Radius Experiment (PREX) [50].

V. SUMMARY

We have studied the isovector dipole response of ^{48}Ca, ^{68}Ni, ^{120}Sn and ^{208}Pb by employing three extended Skyrme interactions that were constructed by fitting the EOSs of asymmetric nuclear matter predicted by chiral effective field theory together with the binding energies of selected closed shell doubly-magic nuclei. We have found that although the RPA calculations using the three extended Skyrme interactions underestimate the peak energy of the giant dipole resonance, they nevertheless well reproduce the experimental data on the electric dipole polarizability.

We have further investigated the correlation between the neutron skin thickness and the product of the electric dipole polarizability and symmetry energy at saturation density. The predicted results from the three extended Skyrme interactions are found to be consistent with the linear relations extracted from RPA calculations using a representative set of energy density functionals. The predicted neutron skin thickness of ^{208}Pb from our study is also consistent with the experimental values [48–50]. Our results thus confirm the usefulness of these extended Skyrme interactions in studying the isovector properties of nuclei in regimes where ab initio calculations with chiral nuclear forces may not be feasible.

Acknowledgements

This work was supported by the US Department of Energy under Contract No. de-sc0015266 and the Welch Foundation under Grant No. A-1358.

[1] P.–G. Reinhard and W. Nazarewicz, Phys. Rev. C **81**, 051303(R) (2010).
[2] J. Piekarewicz, B. K. Agrawal, G. Colò, W. Nazarewicz, N. Paar, P.–G. Reinhard, X. Roca-Maza and D. Vretenar, Phys. Rev. C **85**, 041302(R) (2012).
[3] X. Roca-Maza, M. Brenna, G. Colò, M. Centelles, X. Viñas, B. K. Agrawal, N. Paar, D. Vretenar and J. Piekarewicz, Phys. Rev. C **88**, 024316 (2013).
[4] J. M. Lattimer and A. W. Steiner, Eur. Phys. J. A **50**, 40 (2014).
[5] X. Roca-Maza, X. Viñas, M. Centelles, B. K. Agrawal, G. Colò, N. Paar, J. Piekarewicz and D. Vretenar, Phys. Rev. C **92**, 064304 (2015).
[6] Z. Zhang and L. W. Chen, Phys. Rev. C **90**, 064317 (2014).
[7] Z. Zhang and L. W. Chen, Phys. Rev. C **92**, 031301(R) (2015).
[8] J. Piekarewicz, Eur. Phys. J. A **50**, 25 (2014).
[9] G. Colò, U. Garg, and H. Sagawa, Eur. Phys. J. A **50**, 26 (2014).
[10] C. J. Horowitz and J. Piekarewicz, Phys. Rev. Lett. **86**, 5647 (2001).
[11] F. J. Fattoyev and J. Piekarewicz, Phys. Rev. C **86**, 015802 (2012).
[12] J. Erler, C. J. Horowitz, W. Nazarewicz, M. Rafalski and P.–G. Reinhard, Phys. Rev. C **87**, 044320 (2013).
[13] K. F. Liu and G. E. Brown, Nucl. Phys. **A265**, 385 (1976).
[14] J. Speth and A. van der Woude, Rep. Prog. Phys. 44, 719 (1981).
[15] A. van der Woude, Prog. Part. Nucl. Phys. **18**, 217 (1987).
[16] D. R. Chakrabarty, S. Sen, M. Thoennessen, N. Alamanos, P. Paul, R. Schicker, J. Stachel, and J. J. Gaardhoje, Phys. Rev. C **36**, 1886 (1987).
[17] H. Krivine, J. Treiner, and O. Bohigas, Nucl. Phys. **A336**, 155 (1984).
[18] E. Lipparini, S. Stringari, Phys. Rep. **103**, 1975 (1989).
[19] P. Danielewicz, Nucl. Phys. **A727**, 233 (2003).
[20] J. Meyer, P. Quentin and B. K. Jennings, Nucl. Phys. **A385**, 269 (1982).
[21] L. Trippa, G. Colò, E. Vigezzi, Phys. Rev. C **77**, 061304(R) (2008).
[22] J. Birkhan *et al.*, arXiv:1611.07072 [nucl-ex].
[23] T. Hashimoto *et al.*, Phys. Rev. C **92**, 031305 (2015).
[24] A. Tamii *et al.*, Phys. Rev. Lett. **107**, 062502 (2011).
[25] D. M. Rossi *et al.*, Phys. Rev. Lett. **111**, 242503 (2013).
[26] G. Hagen *et al.*, Nature Phys. **12**, 186 (2016).
[27] M. Miorelli, S. Bacca, N. Barnea, G. Hagen, G. R. Jansen, G. Orlandini and T. Papenbrock, Phys. Rev. C **94**, 034317 (2016).
[28] Y. Lim and J. W. Holt, arXiv:1702.02898 [nucl-th].
[29] C. Wellenhofer, J. W. Holt and N. Kaiser, Phys. Rev. C **93**, 015801 (2015).
[30] C. Wellenhofer, J. W. Holt and N. Kaiser, Phys. Rev. C **93**, 055802 (2016).
[31] B. A. Brown and A. Schwenk, Phys. Rev. C **89**, 011307(R) (2014).
[32] E. Rrapaj, A. Roggero and J. W. Holt, Phys. Rev. C **93**, 065801 (2016).
[33] D. R. Entem and R. Machleidt, Phys. Rev. C **68**, 041001(R) (2003).
[34] L. Coraggio, A. Covello, A. Gargano, N. Itaco, D. R. Entem, T. T. S. Kuo and R. Machleidt, Phys. Rev. C **75**, 024311 (2007).
[35] L. Coraggio, J. W. Holt, N. Itaco, R. Machleidt and F. Sammarruca, Phys. Rev. C **87**, 014322 (2013).
[36] L. Coraggio, J. W. Holt, N. Itaco, R. Machleidt, L. E. Marcucci and F. Sammarruca, Phys. Rev. C **89** 044321 (2014).
[37] E. Chabanat, P. Bonche, P. Haensel, J. Meyer and R. Schaeffer, Nucl. Phys. **A627**, 710 (1997).
[38] B.A. Li, L.W. Chen, and C.M. Ko, Phys. Rep. **464**, 113 (2008).
[39] G. Colò, L.G. Cao, N. Van Giai and L. Capelli, Comput. Phys. Commun. 184, 142 (2013).
[40] A. Leprêtre, H. Beil, R. Bergère, P. Carlos, J. Fagot, A. De Miniac and A. Veyssière, Nucl. Phys. **A367**, 237 (1981).
[41] K. P. Schelhaas, J. M. Henneberg, M. Sanzone-Arenhövel, N. Wieloch-Laufenberg, U. Zurmühl, B. Ziegler, M. Schumacher and F. Wolf, Nucl. Phys. **A489**, 189 (1988).
[42] S. S. Dietrich and B. L. Berman, At. Data Nucl. Data Tables **38**, 199 (1988).
[43] Z. Zhang and L.W. Chen, Phys. Rev. C **93**, 034335 (2016)
[44] J. W. Holt, N. Kaiser, G. A. Miller and W. Weise, Phys. Rev. C **88**, 024614 (2013).
[45] A. Carbone, A. Cipollone, C. Barbieri, A. Rios and Artur Polls, Phys. Rev. C **88**, 054326 (2013).
[46] A. Carbone, A. Rios and A. Polls, Phys. Rev. C **90** 054322 (2014).
[47] J. W. Holt, N. Kaiser and G. A. Miller, Phys. Rev. C **93**, 064603 (2016).
[48] C. M. Tarbert *et al.*, Phys. Rev. Lett. **112**, 242502 (2014).
[49] C. J. Horowitz *et al.*, Phys. Rev. C **85**, 032501(R) (2012).
[50] S. Abrahamyan *et al.*, Phys. Rev. Lett. **108**, 112502 (2012).